

# Dynamic displacement estimation by fusing biased high-sampling rate acceleration and low-sampling rate displacement measurements using two-stage Kalman estimator

Kiyoung Kim, Jaemook Choi, Gunhee Koo and Hoon Sohn\*

*Department of Civil and Environmental Engineering, Korea Advanced Institute of Science and Technology, Daejeon, Republic of Korea*

*(Received December 27, 2015, Revised February 17, 2016, Accepted February 20, 2016)*

**Abstract.** In this paper, dynamic displacement is estimated with high accuracy by blending high-sampling rate acceleration data with low-sampling rate displacement measurement using a two-stage Kalman estimator. In Stage 1, the two-stage Kalman estimator first approximates dynamic displacement. Then, the estimator in Stage 2 estimates a bias with high accuracy and refines the displacement estimate from Stage 1. In the previous Kalman filter based displacement techniques, the estimation accuracy can deteriorate due to (1) the discontinuities produced when the estimate is adjusted by displacement measurement and (2) slow convergence at the beginning of estimation. To resolve these drawbacks, the previous techniques adopt smoothing techniques, which involve additional future measurements in the estimation. However, the smoothing techniques require more computational time and resources and hamper real-time estimation. The proposed technique addresses the drawbacks of the previous techniques without smoothing. The performance of the proposed technique is verified under various dynamic loading, sampling rate and noise level conditions via a series of numerical simulations and experiments. Its performance is also compared with those of the existing Kalman filter based techniques.

**Keywords:** dynamic displacement; two-stage Kalman estimator; multi-rate data fusion

---

## 1. Introduction

Dynamic displacement is one of the most important physical parameters that are crucial to understand dynamic characteristics of vibrating structural systems. Many theoretical approaches aim to calculate the displacement of a structure, and other types of responses can be derived from the displacement. For example, deflection, strain and stress of a structure can be estimated from displacement measurements if the material properties and geometric information are given. Measurement of dynamic displacement is also useful in structural control (Ruiz-Sandoval and Morales 2013) and system identification applications (Jiang and Adeli 2005, Kim *et al.* 2013a, Kim *et al.* 2013b). In addition, displacement measurements have been used for bridge rating (Wang *et al.* 2011), seismic risk assessment (Esposito *et al.* 2014), structural health monitoring (Li *et al.* 2014, He *et al.* 2009, Zhou *et al.* 2013), etc.

---

\*Corresponding author, Professor, E-mail: [hoonsohn@kaist.ac.kr](mailto:hoonsohn@kaist.ac.kr)

In spite of its importance, it is challenging to measure dynamic displacement because displacement is a relative quantity and requires a fixed reference point. One of the most reliable ways to directly measure displacement is to use a linear variable differential transformer (LVDT). However, LVDT requires a direct contact of the device with a target surface at one end, and the other end needs to be firmly fixed to a support. These requirements make the installation of LVDT for field applications challenging. For example, scaffoldings are often required to measure the vertical deflection of a bridge deck, and it becomes even more challenging to measure the lateral deflection. To resolve the limitation, a few noncontact displacement sensors such as GPS, vision based sensor, radar based sensor, FBG sensor and LiDAR (light detection and ranging) have been developed (Tamura *et al.* 2002, Park *et al.* 2007, Kim and Kim 2011, Yang *et al.* 2012, Park *et al.* 2013, Jo *et al.* 2013, Shin *et al.* 2012). However, they still suffer from a low sampling rate, low precision and limited applicability.

Alternatively, displacement is often estimated from the double integration of an acceleration measurement. However, the double integration brings out error accumulation in the displacement due to a bias in the acceleration measurement and integration constant. Since this type of error is unbounded and causes the lack of long-term stability, the treatment of the error is crucial to the accuracy of an estimate (Hong *et al.* 2000, Faruqi and Turner 2000, Yun *et al.* 2012), and there have been several studies to correct the error effectively. For example, baseline correction techniques such as highpass filter (Trifunac 1971), least squares based bias estimation (Chiu 1997), state-space model approach (Gindy *et al.* 2008) and velocity estimation (Park *et al.* 2005), polynomial data fitting (Zhu 2003) and combination of these techniques (Boore 2002) have been proposed, assuming that the displacement has a zero-mean value and the measured acceleration has a linear or polynomial bias. However, when the bias is not a constant, it is hard to properly estimate displacement solely based on the acceleration measurement. Furthermore, these baseline correction techniques do not guarantee convergence to a unique solution (Boore 2001).

Displacement estimation based on multi-rate data fusion augments acceleration data with intermittent displacement measurement to minimize bias accumulation and numerical integration errors during double integration of acceleration. Noncontact sensors such as a global positioning system (GPS) and a vision based sensor, which measure intermittent displacement at a sampling rate lower than the sampling rate of acceleration, can be used to correct bias accumulation and numerical integration errors. For example, GPS can measure displacement at a sampling rate of 4 Hz with the help of RTK technology, and the sampling rate of a vision based sensor is typically limited to 60 Hz due to the frame rate of a video recorder. Chan *et al.* (2006) fused high sampling rate acceleration with low sampling rate GPS displacement using empirical mode decomposition and an adaptive filter. Another study on multi-rate data fusion was conducted by Hong *et al.* (2013). They formulated an optimization problem to estimate displacement based on acceleration and intermittent displacement measurements, and solved the optimization problem in the frequency domain. Park *et al.* (2013) and Cho *et al.* (2015) extracted displacement from strain measurement using the strain-displacement relation calculated from the geometry of a structure, and fused measured acceleration with the extracted displacement by solving the optimization problem proposed by Hong *et al.* (2013). Moschas and Stiros (2010) proposed a filtering technique to de-noise the displacement measured by GPS. First, the filter parameters are selected based on the acceleration measurement, and the filter is applied to GPS displacement to filter out noise components without enhancing the low sampling rate of GPS.

One of the most effective multi-rate data fusion techniques is Kalman filter (Kalman 1960). Contrary to the multi-rate data fusion techniques discussed previously, Kalman filtering explicitly

considers the noise process in measurements and minimizes the uncertainty caused by the noise. Furthermore, Kalman filter enables real-time displacement estimation, and all the necessary parameters of Kalman filter are automatically adjusted without user intervention. Smyth and Wu (2007) formulated a state-space model for multi-rate data fusion by defining only physical responses (i.e., displacement and velocity) as state variables. Because the bias in acceleration measurement is not included in the state-space model, the estimation accuracy deteriorates with a large bias. Kim *et al.* (2014) overcame this problem by constructing a new state-space model for error dynamics. The bias in acceleration measurement and the integration error, which is the sum of numerical integration error and accumulated bias, are estimated from this state-space model. Then, displacement is estimated by subtracting the estimated integration error from the double integration of the acceleration measurement. Due to its direct estimation of the integration error, the technique by Kim *et al.* (2014) is more robust against the bias and noise compared to the technique proposed by Smyth and Wu (2007).

Kalman filter estimates displacement in two steps: prior prediction and posterior correction steps. The prior prediction step is executed every time acceleration is measured, and the acceleration is double integrated through the transition equation of a state-space model. Then, the integration error accumulated during the prior prediction steps is corrected in the posterior correction step where intermittent displacement data becomes available. One major issue with Kalman filter is slow convergence. In the posterior correction step, the posterior estimate of displacement is calculated as a weighted average of the prior displacement estimate and the intermittent displacement measurement. Here, the weighting is a function of Kalman gain, which slowly converges to its steady state value as the number of measurement samples increases. It is well known that the performance of Kalman filter heavily depends on the convergence rate of Kalman gain to the optimal value (Cao and Schwartz 2003). Another problem is discontinuities observed when the posterior correction step is executed intermittently. The integration error is rapidly accumulated during the prior prediction steps and corrected all at once in the posterior prediction step. This sudden correction leads to discontinuities in displacement estimate. When the integration error is large, the discontinuity also increases, deteriorating the accuracy of the displacement estimation.

To further advance Kalman filter based displacement estimation, smoothing algorithms such as fixed point and fixed lag smoothing have been introduced (Rauch 1963, Moore 1973). The fundamental concept of smoothing is to involve additional future measurement data into the displacement estimation at the current time point. By incorporating future measurements into the displacement estimation at the current time point, the convergence rate of Kalman gain is improved and the level of discontinuities is reduced. However, smoothing has its own drawbacks. Firstly, the involvement of additional future measurements results in a time delay in displacement estimation. It is theoretically shown that only 8 time steps of delay are required for 80% improvement in estimation accuracy when measurement noise is very small (Simon 2006). In practice, the typical time delay required for 80% accuracy improvement is, however, much longer than the theoretical value because of high noise level and low sampling rate of commercial noncontact displacement sensors. Another complication is additional computational complexity. Suppose that the size of the state vector is  $m \times 1$ , and  $N$  future measurements are used. Then, fixed point smoothing requires a  $2m \times 1$  state vector and a  $2m \times 2m$  transition matrix, and additional  $N$  recursions to incorporate the future measurements into the estimation of the current state. On the other hand, fixed lag smoothing involves a  $m(N + 1) \times m(N + 1)$  transition matrix and a  $m(N + 1) \times 1$  state vector. Therefore, Kalman filter smoothing requires more memory

spaces and processing time than Kalman filter, especially under high noise and low sampling rate conditions.

This study presents a new dynamic displacement estimation technique based on two-stage Kalman estimator (Friedland 1969, Ignagni 1981) to further improve the accuracy of dynamic displacement. By adopting two-stage Kalman estimator, the proposed technique improves the convergence rate of Kalman gain and minimizes the level of discontinuities without Kalman filter smoothing. The exclusion of smoothing brings out the following two advantages: (1) real time displacement estimation is feasible since no time delay is needed, and (2) memory space and the computational time for displacement estimation are much reduced.

This paper is organized as follows: Section 2 presents a state-space model and a strategy for applying two-stage Kalman estimator to dynamic displacement estimation in the framework of multi-rate data fusion. In Section 3, a series of numerical simulations with varying noise-to-signal ratios (NSR) and sampling rates are performed to examine the performance of the proposed technique. In Section 4, experimental tests using an accelerometer and a laser Doppler vibrometer (LDV) are conducted to verify the effectiveness of the technique in real applications. The major findings and concluding remarks are provided in Section 5.

## **2. Theoretical formulation of two-stage Kalman estimator for dynamic displacement estimation**

In this section, a two-stage Kalman estimator, which deals with state estimation of a dynamic system with an explicit bias in acceleration measurement, is proposed. Conventionally, the bias is included in the state vector of an augmented state-space model, but computational efficiency is compromised by the increased matrix size of the augmented model. Instead of increasing the matrix size, the proposed two-stage Kalman estimator divides the estimation process into two parallel stages which are denoted as Stage 1 and 2, respectively, in this paper.

The overview of data fusion procedure in the proposed technique is shown in Fig. 1. In the proposed technique, an acceleration and a displacement measurement are fused to produce a displacement estimate with high sampling rate, high precision and no integration error. The acceleration measurement has a high sampling rate and precision, but the bias is accumulated through double integration for conversion to displacement. On the other hand, the displacement measurement has a low sampling rate and precision, and its bias can be neglected since no integration is required and bias does not accumulate. In Stage 1, dynamic displacement is estimated without considering the bias. Here, an integration error is only partially corrected, and discontinuities appear in the posterior correction steps of Kalman filter. The Kalman gain obtained in Stage 1 is transferred to Stage 2. In Stage 2, the remaining integration error and the discontinuities in the displacement estimate of Stage 1 are estimated. The final displacement is estimated by subtracting the integration error and discontinuity estimates of Stage 2 from the displacement estimate of Stage 1. In Section 2.1, a state-space model for two-stage Kalman estimator is proposed. The detailed displacement estimation procedure using the two-stage Kalman estimator and the proposed state-space model is discussed in Section 2.2.

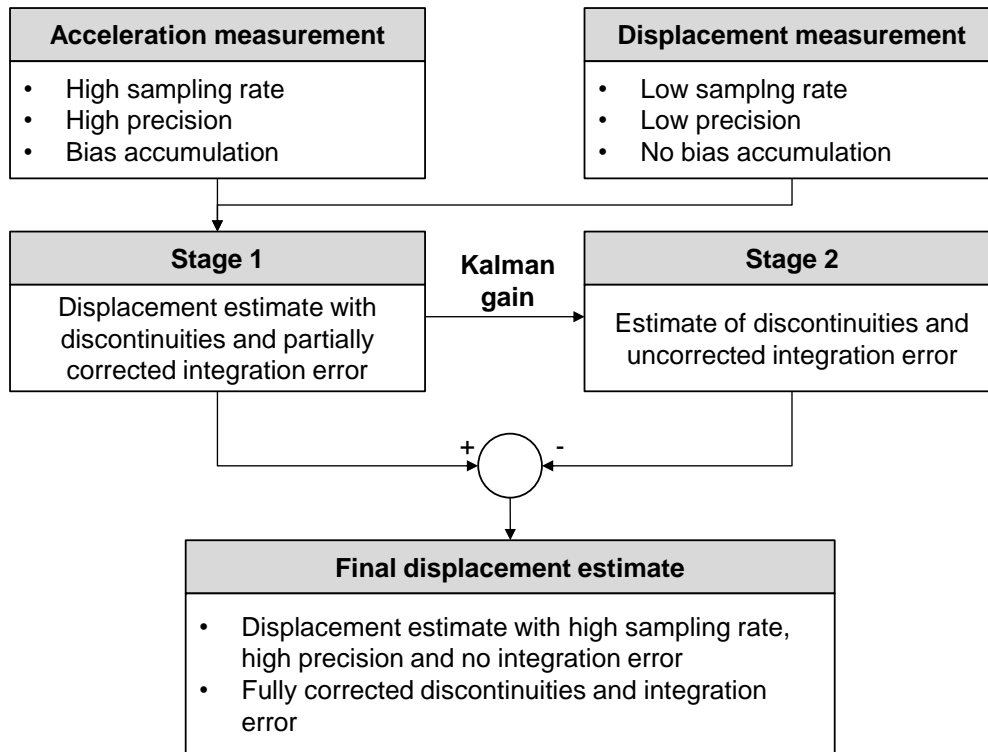


Fig. 1 Overview of the proposed two-stage Kalman estimator technique

### 2.1 Formation of a state-space model

Suppose  $\ddot{x}(k)$ ,  $\dot{x}(k)$  and  $x(k)$  are true acceleration, velocity and displacement at discrete time steps  $k = 0, 1, 2, \dots$ , respectively, and the time increment is  $\Delta t$ . Also, if  $\Delta t$  is small enough,  $\ddot{x}(k)$  can be assumed to be piecewise constant. When a process is piecewise constant, a state (i.e., true acceleration) in a Kalman filter has no system dynamics; i.e.,  $\ddot{x}(k + 1)$  does not differ from  $\ddot{x}(k)$  before a measurement participates in estimation (Rajbhandary and Zhang 2013). Then, the acceleration  $\ddot{x}(k + 1)$  at the time step  $k + 1$  can be expressed as the sum of  $\ddot{x}(k)$  and process noise  $w(k)$

$$\ddot{x}(k + 1) = \ddot{x}(k) + w(k) \tag{1}$$

Then, velocity  $\dot{x}(k + 1)$  is approximated as a discrete integration of  $\ddot{x}(k)$

$$\dot{x}(k + 1) \approx \dot{x}(k) + \ddot{x}(k)\Delta t + w(k)\Delta t \tag{2}$$

Similarly, displacement  $x(k + 1)$  is obtained by double integrating  $\ddot{x}(k)$

$$x(k + 1) \approx x(k) + \dot{x}(k)\Delta t + \frac{1}{2}\ddot{x}(k)\Delta t^2 + \frac{1}{2}w(k)\Delta t^2 \tag{3}$$

Setting up a state vector as  $\mathbf{x}(k) = \{x(k) \quad \dot{x}(k) \quad \ddot{x}(k)\}^T$ , the system transition equation for the double integration process can be constructed by incorporating Eqs. (1)-(3)

$$\mathbf{x}(k+1) = \mathbf{A}\mathbf{x}(k) + \mathbf{B}w(k) \quad (4)$$

where

$$\mathbf{A} = \begin{bmatrix} 1 & \Delta t & \frac{1}{2}\Delta t^2 \\ 0 & 1 & \Delta t \\ 0 & 0 & 1 \end{bmatrix}, \quad \mathbf{B} = \begin{bmatrix} \frac{1}{2}\Delta t^2 \\ \Delta t \\ 1 \end{bmatrix} \quad (5)$$

Note that vectors and matrices are denoted by bold-type characters hereafter.

Let the actual acceleration measurement  $\ddot{x}_m(k)$  and displacement measurement  $x_m(k)$  be sampled at two different intervals  $\Delta t$  and  $N\Delta t$ , respectively. Here,  $N$  is a sampling rate ratio of displacement measurement to acceleration measurement, and this rate is assumed to be an integer greater than 1 in the proposed multi-rate data fusion scheme. The acceleration measurement  $\ddot{x}_m(k)$  can be expressed as the sum of true acceleration  $\ddot{x}(k)$ , zero-mean Gaussian noise  $v_{\ddot{x}}(k)$  and bias  $b(k)$ .

$$\ddot{x}_m(k) = \ddot{x}(k) + v_{\ddot{x}}(k) + b(k) \quad (6)$$

On the other hand, the intermittent displacement measurement  $x_m(k)$  is expressed as the sum of true displacement and zero-mean Gaussian measurement noise  $w_x(k)$

$$x_m(k) = x(k) + w_x(k) \quad (7)$$

When both acceleration and displacement measurements become available ( $k = jN$ ,  $j = 0, 1, 2, \dots$ ) at the posterior correction step (we did not define what posterior correction step is yet), the observation equation is obtained from Eqs. (6) and (7) as follows

$$\mathbf{y}(k) = \mathbf{H}\mathbf{x}(k) + \mathbf{C}b(k) + \mathbf{v}(k) \quad (8)$$

where

$$\mathbf{H} = \begin{bmatrix} 1 & 0 & 0 \\ 0 & 0 & 1 \end{bmatrix}, \quad \mathbf{C} = \begin{bmatrix} 0 \\ 1 \end{bmatrix}, \quad \mathbf{y}(k) = \begin{pmatrix} x_m(k) \\ \ddot{x}_m(k) \end{pmatrix}, \quad \mathbf{v}(k) = \begin{pmatrix} v_x(k) \\ v_{\ddot{x}}(k) \end{pmatrix} \quad (9)$$

On the other hand, when the acceleration measurement is the only observation of the state-space model at the time steps  $k \neq Nj$ , the matrices  $\mathbf{H}$ ,  $\mathbf{C}$ ,  $\mathbf{y}(k)$ ,  $\mathbf{v}(k)$  in Eq. (8) become

$$\mathbf{H} = [0 \quad 0 \quad 1], \quad \mathbf{C} = 1, \quad \mathbf{y}(k) = \ddot{x}_m(k), \quad \mathbf{v}(k) = v_{\ddot{x}}(k) \quad (10)$$

Unlike the state-space models of the previous studies in which the observation equation does not exist when  $k \neq Nj$ , the proposed model accommodates a multi-rate data fusion scheme by changing its observation equation as shown in Fig. 2.

## 2.2 Dynamic displacement estimation using two-stage Kalman estimator

Using the state-space model shown in Eqs. (4) and (8),  $\mathbf{x}(k)$  is estimated using a two-stage Kalman estimator. In Stage 1,  $\mathbf{x}(k)$  is estimated ignoring  $b(k)$ , and Eq. (8) is reduced to the following form

$$\mathbf{y}(k) = \mathbf{H}\mathbf{x}(k) + \mathbf{v}(k) \quad (11)$$

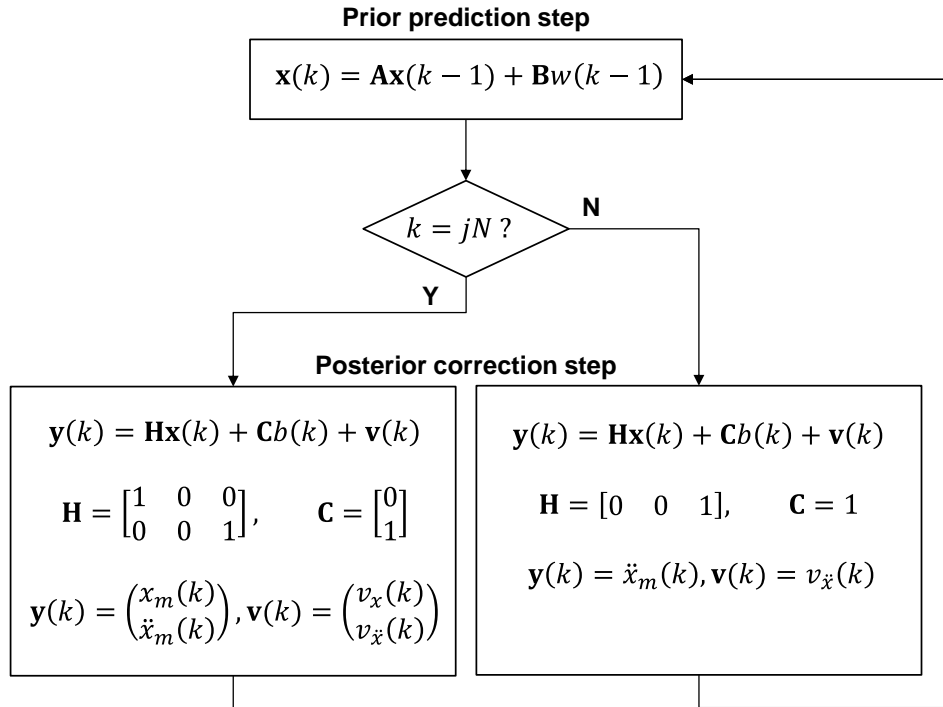


Fig. 2 Multi-rate data fusion scheme based on the proposed state-space model

where  $\mathbf{x}(k)$  is estimated in two steps – prior prediction and posterior correction steps. Define  $\tilde{\mathbf{x}}(k-1)$  as the Stage 1 estimate of  $\mathbf{x}(k-1)$  in the posterior correction step at time step  $k-1$ . In the prior prediction step at time step  $k$ , the prior estimate  $\tilde{\mathbf{x}}^-(k)$  is estimated using Eq. (12), and its uncertainty is expressed using its error covariance matrix  $\mathbf{P}_x^-(k)$  in Eq. (13).

$$\tilde{\mathbf{x}}^-(k) = \mathbf{A}\tilde{\mathbf{x}}(k-1) \tag{12}$$

$$\mathbf{P}_x^-(k) = \mathbf{A}\mathbf{P}_x(k-1)\mathbf{A}^T + \mathbf{Q}(k)\mathbf{B}\mathbf{B}^T \tag{13}$$

where  $\mathbf{P}_x^-(k)$  and  $\mathbf{Q}(k)$  are defined as

$$\mathbf{P}_x^-(k) = E[(\mathbf{x}(k) - \tilde{\mathbf{x}}^-(k))(\mathbf{x}(k) - \tilde{\mathbf{x}}^-(k))^T] \tag{14}$$

$$\mathbf{Q}(k) = E[w(k)w(k)^T] \tag{15}$$

Note that  $\mathbf{Q}(k)$  is identical to the variance of  $w(k)$  because  $w(k)$  is a zero-mean process. Therefore,  $\mathbf{Q}(k)$  is treated as a constant under the assumption of wide-sense stationarity.

In the posterior step, Kalman gain  $\mathbf{K}_x(k)$  is first calculated using Eq. (16). Then,  $\tilde{\mathbf{x}}(k)$  is calculated as a weighted average of  $\tilde{\mathbf{x}}^-(k)$  and  $x_m(k)$  as shown in Eq. (17) with respective weights of  $\mathbf{I} - \mathbf{K}_x(k)\mathbf{H}$  and  $\mathbf{K}_x(k)$ . The posterior error covariance  $\mathbf{P}_x(k)$  in Eq. (18) decreases as  $\mathbf{K}_x(k)$  increases. The covariance matrix  $r(k)$  in Eq. (18) is equivalent to the variance of  $v_x(k)$ , and assumed to be constant similar to  $\mathbf{Q}(k)$ .

$$\mathbf{K}_x(k) = \mathbf{P}_x^-(k)\mathbf{C}^T[\mathbf{H}\mathbf{P}_x^-(k)\mathbf{H}^T + r(k)]^{-1} \tag{16}$$

$$\tilde{\mathbf{x}}(k) = [\mathbf{I} - \mathbf{K}_x(k)\mathbf{H}]\tilde{\mathbf{x}}^-(k) + \mathbf{K}_x(k)\mathbf{y}(k) \quad (17)$$

$$\mathbf{P}_x(k) = E \left[ (\mathbf{x}(k) - \tilde{\mathbf{x}}(k))(\mathbf{x}(k) - \tilde{\mathbf{x}}(k))^T \right] = \mathbf{P}_x^-(k) - \mathbf{K}_x(k)\mathbf{H}\mathbf{P}_x^-(k) \quad (18)$$

$$\mathbf{R}(k) = E[\mathbf{v}(k)\mathbf{v}(k)^T] \quad (19)$$

Note that Stage 1 estimator obtained from Eqs. (14) to (19) is a biased estimator, because  $b(k)$  is ignored in Eq. (11) and  $E[\mathbf{x}(k) - \tilde{\mathbf{x}}(k)]$  is non zero. This implies that the integration errors still remains in Stage 1 estimator, and  $\tilde{\mathbf{x}}(k)$  is biased. Let  $\hat{\mathbf{x}}^-(k)$  and  $\hat{\mathbf{x}}(k)$  the final prior and posterior estimates of  $\mathbf{x}(k)$ . To ensure that  $\hat{\mathbf{x}}^-(k)$  and  $\hat{\mathbf{x}}(k)$  are unbiased, they should be estimated using Eqs. (20) and (21) instead of Eqs. (12) and (17).

$$\hat{\mathbf{x}}^-(k) = \mathbf{A}\hat{\mathbf{x}}(k-1) \quad (20)$$

$$\hat{\mathbf{x}}(k) = \hat{\mathbf{x}}^-(k) + \mathbf{K}_x(k)[\mathbf{y}(k) - \mathbf{H}\hat{\mathbf{x}}^-(k) - \mathbf{C}b(k)] \quad (21)$$

Note that  $\mathbf{K}_x(k)$  is not influenced by  $b(k)$ , since  $\mathbf{P}_x^-(k)$  and  $\mathbf{P}_x(k)$  in Eqs. (14) and (18) do not change as long as the initial value of  $\mathbf{P}_x(k)$  is identical. Therefore,  $\mathbf{K}_x(k)$  obtained in Stage 1 can be directly used in Eq. (21).

In Stage 2,  $\hat{\mathbf{x}}(k)$  and  $\tilde{\mathbf{x}}(k)$  are assumed to be related to each other as follows

$$\hat{\mathbf{x}}^-(k) = \tilde{\mathbf{x}}^-(k) + \mathbf{U}(k)b(k) \quad (22)$$

$$\hat{\mathbf{x}}(k) = \tilde{\mathbf{x}}(k) + \mathbf{V}(k)b(k) \quad (23)$$

where  $\mathbf{U}(k)$  and  $\mathbf{V}(k)$  are  $2 \times 1$  prior and posterior sensitivity matrices, which need to be estimated at time step  $k$ .

$\mathbf{U}(k)$  and  $\mathbf{V}(k)$  can be estimated through a recursion process using  $\mathbf{K}_x(k)$  as follows. Substituting Eqs. (12) and (20) into Eq. (22) produces the following recursive equation

$$\mathbf{U}(k) = \mathbf{A}\mathbf{V}(k-1) \quad (24)$$

Similarly, another recursive equation is obtained by substituting Eqs. (17) and (21) into Eq. (23).

$$\mathbf{V}(k) = \mathbf{U}(k) - \mathbf{K}_x(k)\mathbf{S}(k) \quad (25)$$

where  $\mathbf{S}(k) = \mathbf{H}\mathbf{U}(k) + \mathbf{C}$ . Eqs. (24) and (25) construct a recursion process for obtaining  $\mathbf{U}(k)$  and  $\mathbf{V}(k)$  using  $\mathbf{K}_x(k)$ .

Once  $\mathbf{U}(k)$  and  $\mathbf{V}(k)$  are estimated,  $b(k)$  is estimated using the relation made in Eqs. (22) and (23). Let us define the measurement residual,  $\mathbf{r}(k)$ , as

$$\mathbf{r}(k) = \mathbf{y}(k) - \mathbf{H}\hat{\mathbf{x}}^-(k) \quad (26)$$

Then, substituting Eq. (22) into Eq. (26) results in an observation equation of another state-space model.

$$\mathbf{r}(k) = \mathbf{S}(k)b(k) + \mathbf{z}(n) \quad (27)$$

where  $\mathbf{z}(n)$  is another zero-mean Gaussian random process defined as  $\mathbf{z}(n) = \mathbf{y}(k) - \mathbf{C}\hat{\mathbf{x}}^-(k)$ , and its covariance matrix is calculated as  $\mathbf{C}\tilde{\mathbf{P}}_x^-(k)\mathbf{C}^T + \mathbf{r}(k)$ . Suppose  $b(k)$  is a piecewise constant process without noise (i.e.,  $b(k) = b(k-1)$ ). Then, the recursive Kalman filter for the estimation of  $b(k)$  is summarized as

$$\hat{b}^-(k) = \hat{b}(k-1) \quad (28)$$

$$P_b^-(k) = P_b(k-1) \quad (29)$$

$$\mathbf{K}_b(k) = P_b^-(k)\mathbf{S}^T(k)[\mathbf{H}\mathbf{P}_x^-(k)\mathbf{H}^T + \mathbf{S}(k)P_b^-(k)\mathbf{S}^T(k) + \mathbf{R}(k)]^{-1} \quad (30)$$

$$\hat{b}(k) = (\mathbf{1} - \mathbf{K}_b(k)\mathbf{S}(k))\hat{b}^-(k) + \mathbf{K}_b(k)\mathbf{r}(k) \quad (31)$$

$$P_b(k) = P_b^-(k) - P_b^-(k)\mathbf{K}_b(k)\mathbf{S}(k) \quad (32)$$

where  $\hat{b}^-(k)$  and  $\hat{b}(k)$  are the prior and posterior estimates of  $b(k)$ , respectively, and  $P_b^-(k)$  and  $P_b(k)$  are the error covariance matrices of the prior and posterior estimations, respectively. Also,  $\mathbf{K}_b(k)$  is the Kalman gain of the bias estimation.

Finally,  $\hat{\mathbf{x}}(k)$  is obtained by replacing  $b(k)$  in Eq. (27) with  $\hat{b}(k)$  obtained from Eq. (23)

$$\hat{\mathbf{x}}(k) = \tilde{\mathbf{x}}(k) + \mathbf{V}(k)\hat{b}(k) \quad (33)$$

Note that Stage 2 cannot be executed without  $\mathbf{K}_x(k)$ . Since  $\mathbf{K}_x(k)$  is acquired at the posterior correction step, a state-space model for two-stage Kalman estimator needs to have an observation equation at every time step. The state-space models proposed in the previous studies do not have observation equation when  $k \neq Nj$ , and two-stage Kalman estimator can be applied only when intermittent displacement data are measured. However, using the proposed state-space model in this study,  $\mathbf{V}(k)$  and  $\hat{b}(k)$  in Eq. (32) can be updated continuously, and this is a major advantage of the proposed technique in terms of accuracy enhancement. The process of two-stage Kalman estimator is summarized in Fig. 3.

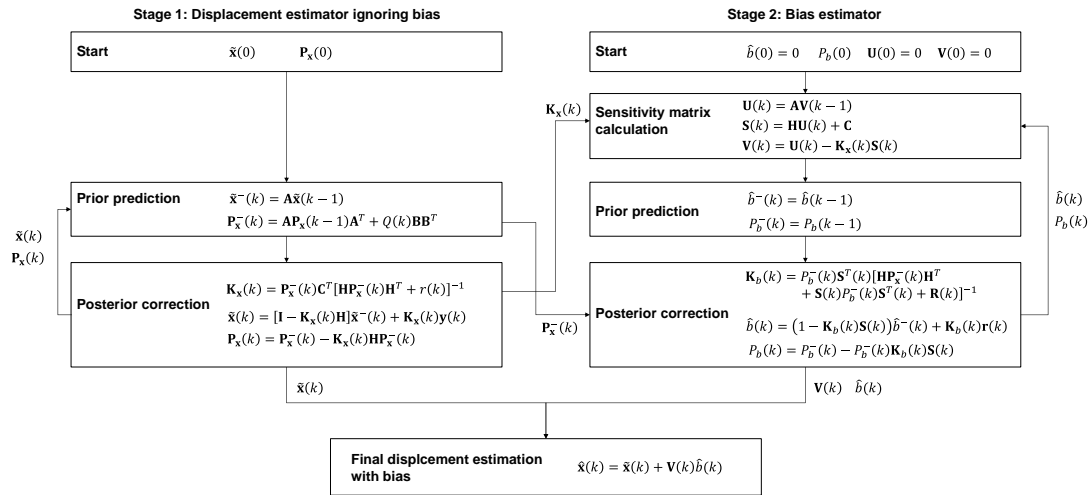


Fig. 3 Two-stage Kalman estimator for displacement estimation

### 3. Numerical simulation

A series of numerical simulations were conducted using a 3-DOF spring-mass system in Fig. 4

(a) with various noise conditions and sampling rates.  $m_1$ ,  $m_2$  and  $m_3$  are set to 100 kg, and  $k_1$ ,  $k_2$  and  $k_3$  are set to 40426, 20213, 1579.1 N/m, so that the undamped natural frequencies of the system are 0.59, 1.84 and 4.19 Hz. All the damping coefficients,  $c_1$ ,  $c_2$  and  $c_3$ , are set to 30 N/m-sec. The accelerogram recorded during Tohoku earthquake was applied to the support next to  $m_1$  and denoted as  $\ddot{y}(t)$ . The accelerogram was measured in E-W direction at Tsukidate (MYG004) station for 300 seconds with a sampling rate of 100Hz. However, only the initial 150 second record was used in this study (Fig. 4(b)), since acceleration and displacement are negligible after 150 second.

The accelerations  $\ddot{x}_1$ ,  $\ddot{x}_2$  and  $\ddot{x}_3$  and displacements  $x_1$ ,  $x_2$  and  $x_3$  of the three masses shown in Fig. 5 are calculated using discrete-time state-space equations under the zero-order hold condition (Chen 1999) and the same sampling rate as the base acceleration. The calculated displacements are used as the reference values for later comparison with estimated values. Acceleration responses measured by accelerometers are simulated by adding zero-mean Gaussian white noise and bias components to the previous reference responses in Fig. 5(a). The white noises are added so that all simulated acceleration measurements have NSR (noise-to-signal ratio) of 0.1%. In addition, the simulated acceleration responses are adjusted to have  $-5 \text{ mm/sec}^2$  bias, which is identical to the bias in the base accelerogram in Fig. 4(b). The sampling rate of the simulated acceleration measurements is unchanged from the sampling rate of the reference signals.

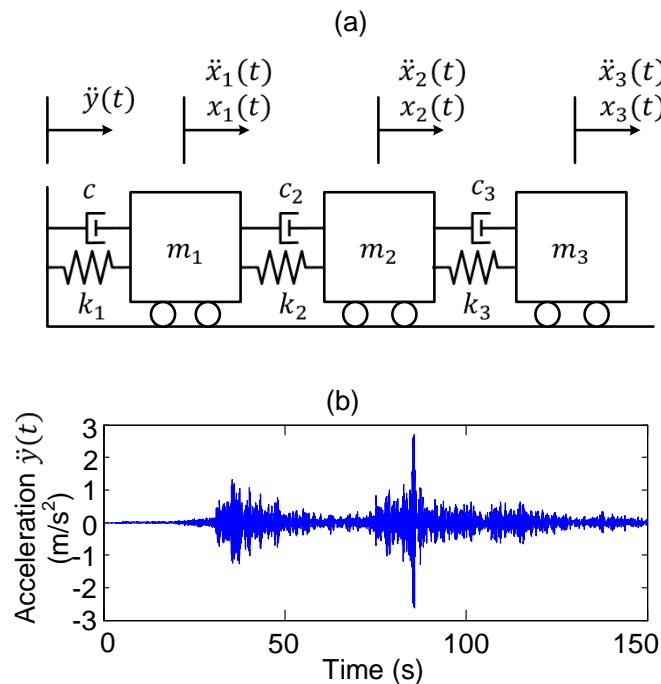


Fig. 4 Structure and external input used in numerical simulations: (a) 3-DOF spring-mass system and (b) Base acceleration signal  $\ddot{y}(t)$  from Tohoku earthquake, Japan, 2011

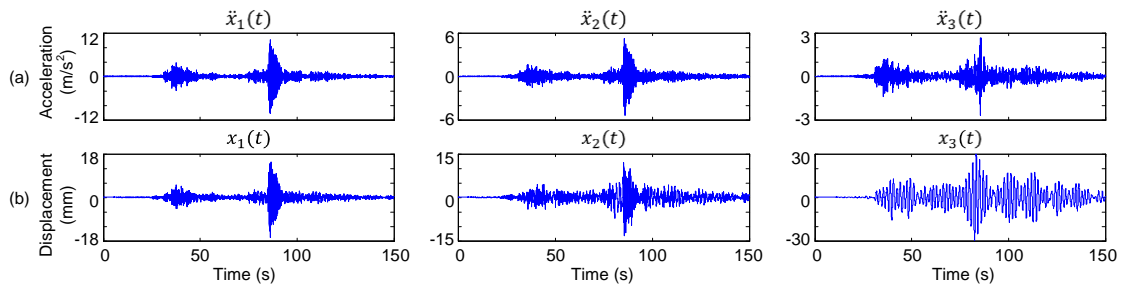


Fig. 5 Reference acceleration and displacement responses of the 3-DOF system obtained by numerical simulations: (a) acceleration responses  $\ddot{x}_1$ ,  $\ddot{x}_2$  and  $\ddot{x}_3$  and (b) displacement responses  $x_1$ ,  $x_2$  and  $x_3$

For the simulation of displacement measurements, a total of 25 signals are simulated at each DOF by varying NSR and the sampling rate. The NSR value is varied from 0 to 0.5, 1.0, 1.5 and 2.0 %, and the sampling rate from 10 to 5, 3.3, 2.5, 2 Hz. These sampling rates are equivalent to  $N$  values of 10, 20, 30, 40 and 50, respectively. Bias in the displacement measurement is not considered because its contribution to displacement estimation is negligible. When the precision and sampling rate of typical laser distance-meters (2-3 mm precision, and below 10 Hz sampling rate) are considered, the characteristics of these laser distance-meters are similar to the simulation case with  $N = 10$  and NSR = 1.0% (Blais 2004).

The performance of the proposed technique is compared with those of the previous techniques proposed by Smyth and Wu (2007) and Kim *et al.* (2014), which are denoted as Technique I and Technique II respectively hereafter. Note that Techniques I and II include online and offline smoothing algorithms, respectively. However, the smoothing algorithms in these techniques are not included in the accuracy comparison of the three techniques performed in this study. The smoothing algorithms are applied to Techniques I and II only when the computational times for achieving the same level of accuracy as the proposed technique are compared.

The displacement estimation performances of the proposed technique, Techniques I and II are compared. Fig. 6 shows the root mean square (RMS) error between the displacement estimated by one of these estimation techniques and the reference displacement. The RMS error of the proposed technique is smaller than those of Techniques I and II. Even for the worst case scenario (i.e.,  $N = 50$  and NSR = 2%), the RMS error of the proposed technique does not exceed 0.25 mm, which corresponds to 4.26% of the overall response level. On the other hand, the RMS error of Technique I rapidly increases as NSR and  $N$  increase. (Fig. 6(a)). This indicates that the estimate of Technique I is more sensitive to both NSR and  $N$  than the other techniques. Technique II is less sensitive to  $N$  and NSR, but its estimation accuracy is not as good as that of the proposed technique.

One of the advantages of the proposed technique is that it reduces the RMS error especially at the beginning of the estimated displacement signal compared to Techniques I and II. As discussed in Section 1, the estimation error at the beginning of the time signal can not only deteriorate estimation accuracy, but also result in a permanent drift especially when NSR and  $N$  are high. In Fig. 7(a), Technique I produces a drift error, since the estimation error at the beginning of the displacement estimate is accumulated during estimation. Also, Technique II shows a higher initial estimation error than the proposed technique, as shown in Figs. 7(b) and 7(c).

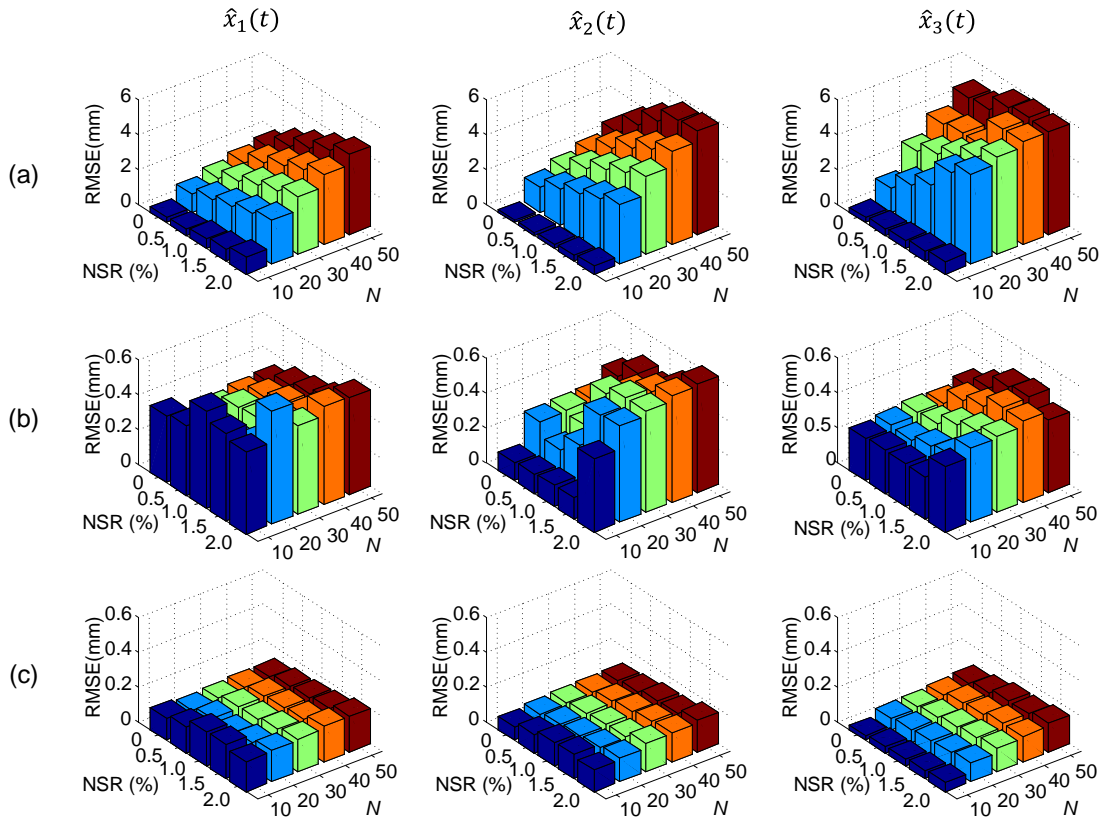


Fig. 6 RMS error between the reference displacement and the displacement estimated by (a) Technique I, (b) Technique II, and (c) the proposed technique

Next, the computational times of the techniques required to achieve the same level of displacement accuracy are compared. In the comparison, CPU times of the proposed technique are first measured without smoothing using MATLAB in a 64 bit computer environment for all cases. Then, CPU times of Techniques I and II incorporated with online Rauch-Tung-Striebel (RTS) smoothing algorithm are measured for the same cases. Here, the time delays for the smoothing algorithm are determined so that the RMS errors of Techniques I and II are closest to that of the proposed technique. Considering the average of all compared cases, the CPU time of the proposed technique is 0.526 second on average, while the CPU times of the Techniques I and II are 1.258 and 0.865 sec. The result indicates that the proposed technique reduces the CPU time by 58.2% and 39.2% compared to those of Techniques I and II, respectively.

Because the acceleration bias at the beginning of the estimate is double integrated and affects the displacement estimation, the bias error accumulates over time in the displacement estimate, and produces a permanent drift error. Therefore, it is also important to make sure that the estimated bias value converges to the exact one as soon as possible. Fig. 8 shows the bias estimated by the proposed technique converges to the exact bias value of  $-5 \text{ mm/s}^2$  faster than the bias estimated by Technique II.

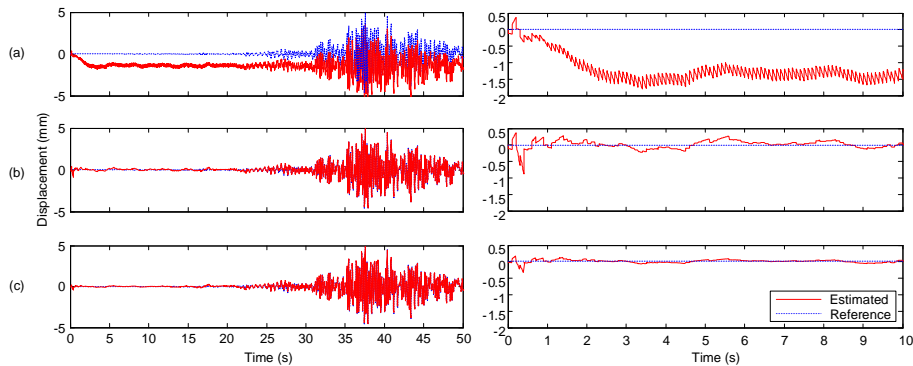


Fig. 7 Displacement  $x_1$  estimated by (a) Technique I, (b) Technique II and (c) the proposed technique (left) and their magnified plots in 0 to 10 s (right), when  $N = 10$  and NSR = 1%

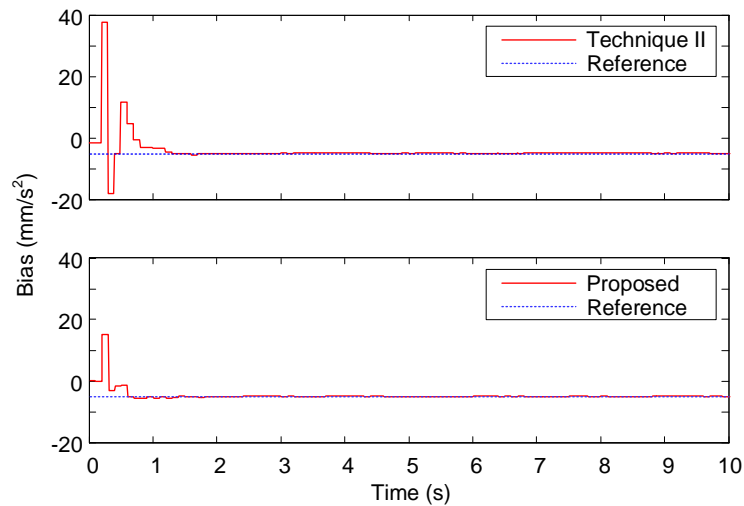


Fig. 8 The bias estimated by (a) Technique II and (b) the proposed technique

Another advantage of the proposed technique is that it alleviates sudden discontinuities at the posterior correction steps where estimates are corrected by intermittent displacement measurements. The discontinuities are unavoidable in the previous techniques, and the only remedy to remove the discontinuities is the application of a smoothing algorithm, which raises the other problems as discussed in Section 1. Fig. 9 shows the discontinuities in the displacement estimated by the three techniques when no smoothing algorithm is applied. Technique I shows the highest level of discontinuities. The sudden discontinuities are reduced in Technique II, because the bias estimate remains constant and does not grow until the next posterior correction step. By estimating the bias more precisely and faster in Stage 2, the proposed technique further lessens the discontinuities successfully. The RMS errors for Techniques I and II and the proposed technique are 0.87, 0.17, 0.15 mm, respectively.

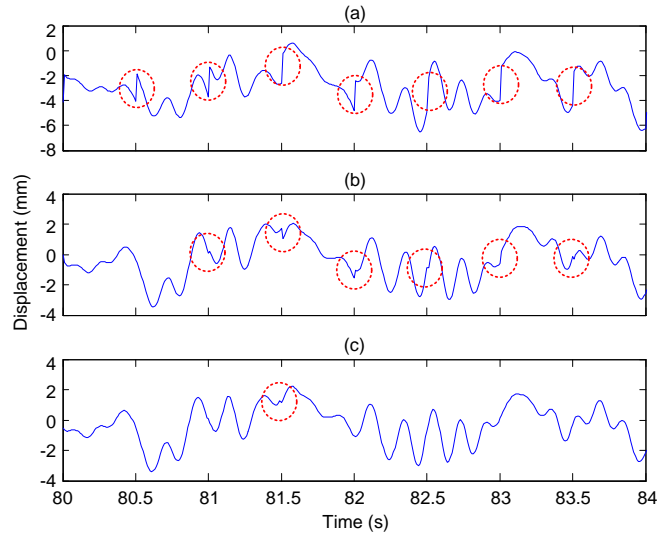


Fig. 9 Discontinuities in the displacement observed at the posterior correction time steps (marked with dashed circles) by (a) Technique I, (b) Technique II and (c) the proposed technique. ( $x_2$ ,  $N = 50$  and NSR = 0.5%)

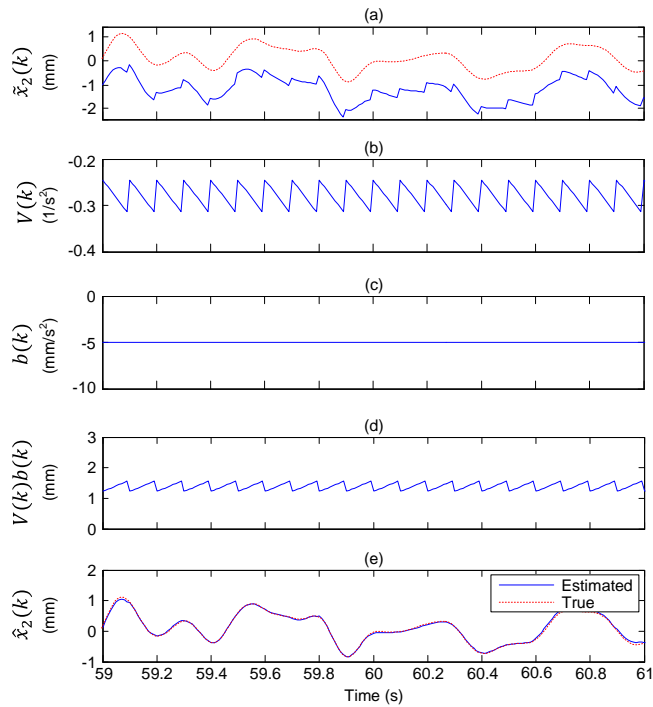


Fig. 10 Before explaining each subfigure. We need an overall description of Fig 10: (a) Displacement estimate in Stage 1, (b)  $V(k)$  estimate in Stage 2, (c) bias estimate in Stage 2, (d) the product of bias and discontinuities ( $V(k)b(k)$ ), and (e) the final estimate of displacement ( $\hat{x}_2(k) - V(k)b(k)$ )

Fig. 10 shows the estimation results of Stages 1 and 2 and the final displacement estimate obtained by the proposed technique. Stage 1 estimates the displacement, which is technically the same as the estimate of Technique I, since both estimators do not consider the bias in acceleration measurement. Similar to Fig. 7(a), the displacement estimate of Stage 1 has a permanent drift error and discontinuities as shown in Fig. 10(a). However, Stage 2 precisely estimates not only the drift error but also the discontinuities. Figs. 10(b) and 10(c) shows  $\mathbf{V}(k)$  and  $b(k)$  estimated in Stage 2. Here, the discontinuities and the bias in acceleration measurement are effectively estimated through  $\mathbf{V}(k)$  and  $b(k)$ . As a result, the error in Stage 1 is estimated as the form of  $\mathbf{V}(k)b(k)$  (Fig. 10(d)), and removed from Stage 1 estimate for the final displacement estimate (Fig. 10(e)).

#### 4. Experimental verification

A series of experiments were conducted to verify the performance of the proposed technique for various types of displacements in practice. The structure and sensors used in the experiments are shown in Fig. 11. Target displacement was measured from a cantilever beam, which has a dimension of 40 cm × 2 cm × 2 mm and made of mild steel. A mass of 0.21 kg is attached on the top of the beam, and the displacement of the mass is measured. APS 400 Electro-seis vibration exciter is connected to the beam via a slender steel rod. A PCB Piezotronics 352C33 accelerometer, which has a mass of 21.8 g including the mass of its magnet mount, is attached on the mass for acceleration measurement. To measure displacement of the mass, Polytec PSV-400 scanning vibrometer is used. This laser Doppler vibrometry (LDV) emits a laser beam to the opposite side of the mass where the accelerometer is attached. The displacement measured by Optex-FA CD-4 350 laser displacement sensor (LDS), which is installed on the same side as the accelerometer, is used as the reference (ground true) displacement. The sampling rate of the accelerometer and the LDS is set to 1280 Hz. On the other hand, the displacement measured by LDV is down sampled at 128 Hz ( $N = 10$ ) to mimic the low sampling rate of other typical noncontact displacement sensors such as GPS and commercial laser distance-meter.

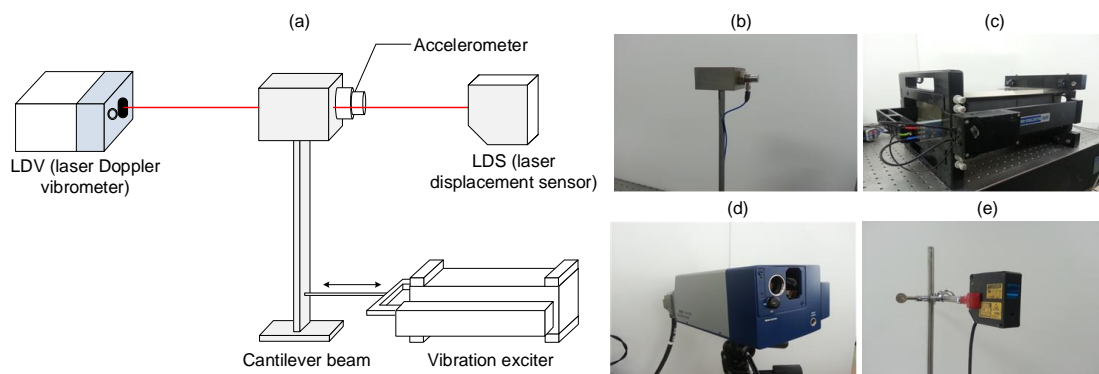


Fig. 11 Sensors and actuator used in the experiments: (a) overall configuration, (b) cantilever beam and accelerometer, (c) vibration exciter, (d) LDV and (e) LDS

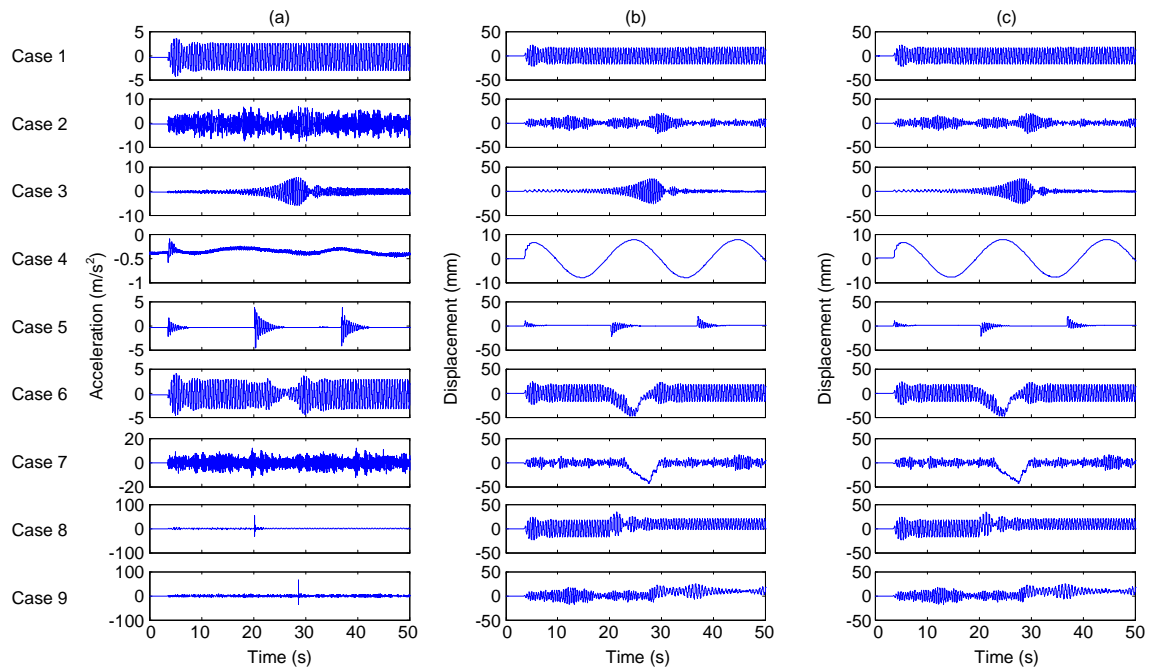


Fig. 12 The measured acceleration and displacement responses corresponding to nine different loading cases: (a) measured acceleration, (b) LDV displacement measurement and (c) LDS displacement measurement

Table 1 Loading cases in the experiments

| Loading case | Description   |
|--------------|---|
| 1            | 2 Hz sinusoidal excitation  |
| 2            | Random excitation with 0 – 20 Hz frequency band                     |
| 3            | Chirp excitation of 1 – 8 Hz  |
| 4            | 0.05 Hz sinusoidal excitation to represent pseudo-static excitation |
| 5            | Impulse excitation  |
| 6            | 2Hz sinusoidal excitation + pseudostatic excitation                 |
| 7            | Random excitation + pseudostatic excitation                         |
| 8            | 2Hz sinusoidal excitation + permanent displacement                  |
| 9            | Random excitation + permanent displacement                          |

The dynamic response of the mass is generated by exciting the cantilever beam using the vibration exciter. Nine different loading cases are generated as shown in Table 1. Each loading case is designed carefully to verify the performance of the proposed technique. A sinusoidal input is applied to the beam in Case 1. Cases 2 and 3 are designed to examine the performance of the proposed technique for a broadband frequency range. Pseudo-static and impact loadings are applied in Cases 4 and 5, respectively. Mixtures of dynamic and pseudo-static loadings are applied in Cases 6 to 9. Here, pseudo-static loadings are generated by pushing the mass manually, and the permanent displacements shown in Cases 8 and 9 are formed by removing rubber bands which provide restoration force to the vibration exciter and applying manual force to the vibrating part of the exciter. Note that the displacements corresponding to loading Cases 4 to 9 may have nonzero mean displacements, which do not satisfy the assumptions made in the baseline correction and displacement reconstruction techniques mentioned in Section 1. Fig. 12 presents the acceleration records measured by the accelerometer and the displacements measured by LDV and LDS.

Fig. 13 demonstrates that the proposed technique closely trace the reference displacements in all loading cases despite of the nonzero-mean displacement. Table 2 compares the RMS error of the proposed technique with the ones by Techniques I and II. The RMS error of the proposed technique is reduced by 86% and 57% compared to the RMS errors of Technique I and II, respectively. Technique I does not estimate the displacement properly due to its limitation discussed in Section 3. Also, Technique II makes less accurate estimates than the proposed technique, because of its relatively high initial estimation error and remaining discontinuities. Fig. 14 shows that the initial overshooting of the bias estimate is significantly reduced when the proposed technique is used over Technique II. The reduction of this bias error has the biggest contribution to the performance improvement of the proposed techniques as illustrated in Table 2.

Table 2 Comparison of the RMS errors and relative errors of the displacements estimated by three techniques

| Case #     | Technique I       |      | Technique II   |     | Proposed technique |     |
|------------|-------------------|------|----------------|-----|--------------------|-----|
|            | RMS error<br>(mm) | (%)  | RMS error (mm) | (%) | RMS error<br>(mm)  | (%) |
| 1          | 0.937             | 621  | 0.293          | 194 | 0.151              | 100 |
| 2          | 0.364             | 1916 | 0.035          | 184 | 0.019              | 100 |
| 3          | 0.247             | 1300 | 0.039          | 205 | 0.019              | 100 |
| 4          | 0.185             | 370  | 0.098          | 196 | 0.050              | 100 |
| 5          | 0.287             | 2870 | 0.022          | 220 | 0.010              | 100 |
| 6          | 0.410             | 423  | 0.160          | 165 | 0.097              | 100 |
| 7          | 0.246             | 273  | 0.010          | 111 | 0.009              | 100 |
| 8          | 2.400             | 764  | 0.979          | 312 | 0.314              | 100 |
| 9          | 0.446             | 314  | 0.204          | 144 | 0.142              | 100 |
| <b>Avg</b> | 0.614             | 714  | 0.199          | 231 | 0.086              | 100 |

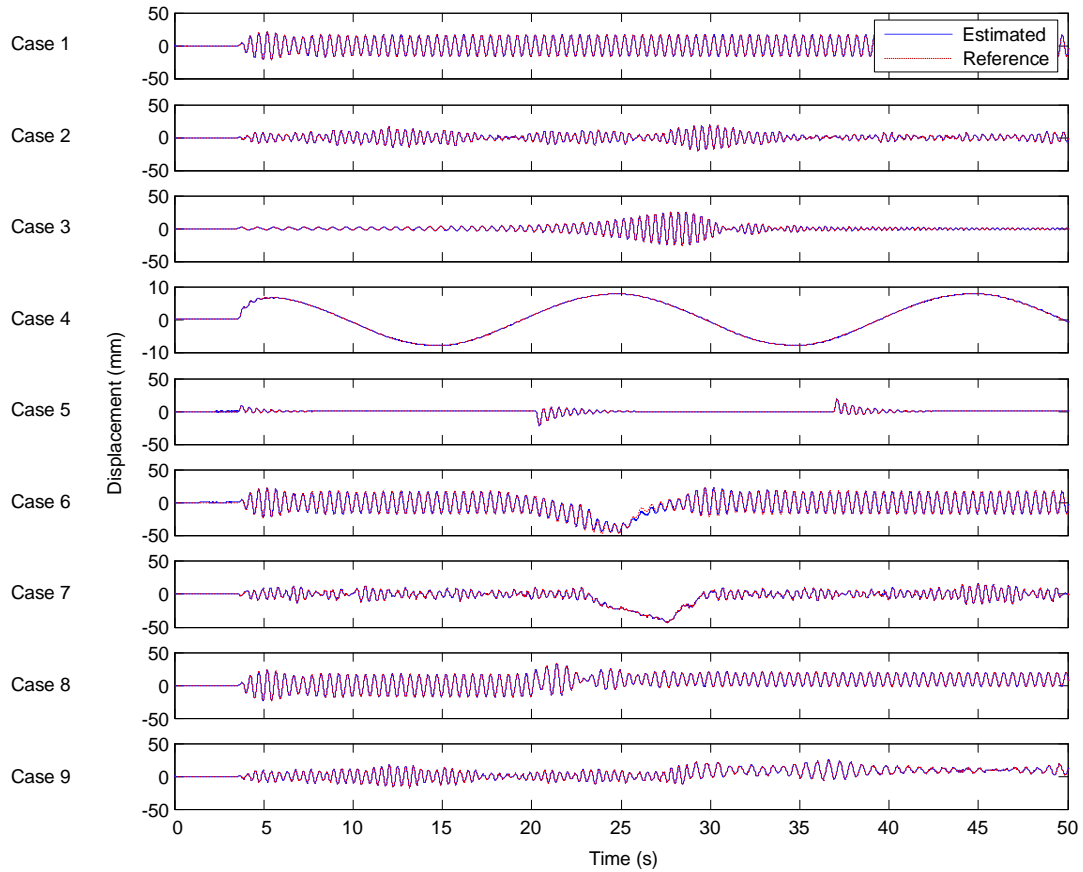


Fig. 13 Comparison of the displacements estimated by the proposed technique and the reference displacements measured by LDS

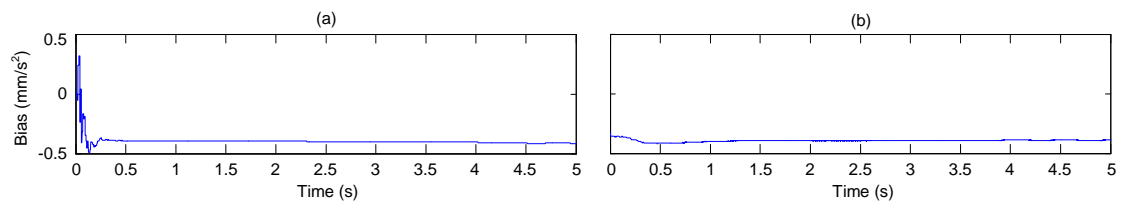


Fig. 14 Comparison of the bias estimated for Case 4 by (a) Technique II and (b) the proposed technique

## 5. Conclusions

This study presents a two-stage Kalman estimator, which estimates high-accuracy dynamic displacement by combining high-sampling rate acceleration data with low-sampling rate displacement measurement. The proposed technique (1) effectively reduces the estimation error

particularly at the beginning of the estimated displacement time signal and the resultant permanent drift error, (2) allows faster convergence of the estimated bias in acceleration measurement into the true value, (3) minimizes the signal discontinuities in the estimated displacement at the posterior correction steps where intermitted displacement is measured, and (4) allows real-time dynamic displacement estimation without smoothing. The performance of the proposed technique is verified and compared with the performance of the previous Kalman filter based techniques under various conditions via a series of numerical simulations and experiments. When the proposed technique is applied to experimental test data obtained from a cantilever beam, the accuracy of the displacement estimation is improved by 86% and 57% compared to the ones estimated by Technique I (Smyth and Wu 2007) and II (Kim *et al.* 2014), respectively.

## Acknowledgements

This research was supported by a grant (15CTAP-C097371-01) from Technology Advancement Research Program (TARP) funded by Ministry of Land, Infrastructure and Transport of Korean government.

## References

- Boore, D.M. (2001), "Effect of baseline corrections on displacement and response spectra for several recordings of the 1999 Chi-Chi, Taiwan, earthquake", *B. Seismol. Soc. Am.*, **91**(5), 1199-1211.
- Boore, D.M., Stephens, C.D. and Joyner, W.B. (2002), "Comments on baseline correction of digital strong-motion data: examples from the 1999 Hector Mine, California, earthquake", *B. Seismol. Soc. Am.*, **92**(4), 1543-1560.
- Cao, L. and Schwarz, H.M. (2003), "Exponential convergence of the Kalman filter based parameter estimation algorithm", *Int. J. Adapt. Control*, **17**(10), 763-783.
- Chan, W.S., Xu, Y.L., Ding, X.L. and Dai, W.J. (2006), "An integrated GPS-accelerometer data processing technique for structural deformation monitoring", *J. Geodesy*, **80**(12), 705-719.
- Chiu, H.C. (1997), "Stable baseline correction of digital strong-motion data", *B. Seismol. Soc. Am.*, **87**(4), 932-944.
- Cho, S., Yun, C.B. and Sim, S.H. (2015), "Displacement estimation of bridge structures using data fusion of acceleration and strain measurement incorporating finite element model", *Smart Struct. Syst.*, **15**(3), 645-663.
- Esposito, S., Iervolino, I., d'Onofrio, A. and Santo, A. (2014), "Simulation-based seismic risk assessment of gas distribution networks", *Comput. - Aided Civ. Inf.*, doi: 10.1111/mice.12105.
- Faruqi, F.A. and Turner, K.J. (2000), "Extended Kalman filter synthesis for integrated global positioning / inertial navigation systems", *Appl. Math. Comput.*, **115**(2-3), 213-227.
- Gindy, M., Vaccaro, R. Nassif, H. and Velde, J. (2008), "A state-space approach for deriving bridge displacement from acceleration", *Comput. - Aided Civ. Inf.*, **23**(4), 281-290.
- He, W., Wu., Zhishen, Kojima, Y. and Asakura, T. (2009), Failure mechanism of deformed concrete tunnels subject to diagonally concentrated load, *Comput. - Aided Civ. Inf.*, **24**(6), 416-431.
- Hong, S., Lee, M., Rios, J. and Speyer, J.L. (2000), "Observability analysis of GPS aided INS", *Proceedings of the 13th International Technical meeting of the Satellite Division of the Institute of Navigation (ION GPS 2000)*, Sep. 19-22, 2000, Salt Lake City, UT.
- Hong, Y.H., Kim, H. and Lee, H.S. (2013), "Design of the FEM-FIR filter for displacement reconstruction using accelerations and displacements measured at different sampling rates", *Mech. Syst. Signal Pr.*, **38**(2),

- 460-481.
- Jiang, X. and Adeli, H. (2005), "Dynamic wavelet neural network for nonlinear identification of highrise buildings", *Comput. - Aided Civ. Inf.*, **20**(5), 316-330.
- Jo, H., Sim, S.H., Tatkowski, A., Spencer, Jr., B.F. and Nelson, M.E. (2013), "Feasibility of displacement monitoring using low-cost GPS receivers", *Struct. Control Health Monit.*, **20**(9), 1240-1254.
- Kalman, R.E. (1960), "A new approach to linear filtering and prediction problems", *J. Basic Eng.*, **82**(1), 35-45.
- Kim, J., Kim, K. and Sohn, H. (2013a), "Data-driven physical parameter estimation for lumped mass structures from a single point actuation test", *J. Sound Vib.*, **332**(18), 4390-4402.
- Kim, J., Kim, K. and Sohn, H. (2013b), "In situ measurement of structural mass, stiffness, and damping using a reaction force actuator and a laser Doppler vibrometer", *Smart Mater. Struct.*, **22**(8), 085004.
- Kim, J., Kim, K. and Sohn, H. (2014), "Autonomous dynamic displacement estimation from data fusion of acceleration and intermittent displacement measurements", *Mech. Syst. Signal Pr.*, **42**(1-2), 194-205.
- Kim, S.W. and Kim, N.S. (2011), "Multi-point displacement response measurement of civil infrastructures using digital image processing", *Procedia Eng.*, **14**, 195-203.
- Li, J., Hao, H., Fan, K. and Brownjohn, J. (2014), "Development and application of a relative displacement sensor for structural health monitoring of composite bridges", *Struct. Control Health Monit.*, DOI: 10.1002/stc.1714.
- Moore, J.B. (1973), "Discrete-time fixed-lag smoothing algorithms", *Automatica*, **9**(2), 163-173.
- Moschas, F. and Stiros, S. (2011), "Measurement of dynamic displacements and of the modal frequencies of a short-span pedestrian bridge using GPS and an accelerometer", *Eng. Struct.*, **33**(1), 10-17.
- Park, H.S., Lee, H.M., Adeli, H. and Lee, I. (2007), "A new approach for health monitoring of structures: terrestrial laser scanning", *Comput. - Aided Civ. Inf.*, **22**(1), 19-30.
- Park, H.S., Son, S., Choi, S.W. and Kim, Y. (2013), "Wireless laser range finder system for vertical displacement monitoring of mega-trusses during construction", *Sensors*, **13**(5), 5796-5813.
- Park, J.W., Sim, S.H. and Jung, H.J. (2013), "Displacement estimation using multimetric data fusion", *IEEE/ASME T. Mechatronics*, **18**(6), 1675-1682.
- Park, K.T., Kim, S.H., Park, H.S. and Lee, K.W. (2005), "The determination of bridge displacement using measured acceleration", *Eng. Struct.*, **27**(3), 371-378.
- Rauch, H.E. (1963), "Solutions to the linear smoothing problem", *IEEE T. Automat Contr.*, **8**(4), 371-372.
- Ruiz-Sandoval, M.E. and Morales, E. (2013), "Complete decentralized displacement control algorithm", *Smart Struct. Syst.*, **11**(2), 163-183.
- Shin, S., Lee, S.U. and Kim, N.S. (2012), "Estimation of bridge displacement responses using FBG sensors and theoretical mode shapes", *Struct. Eng. Mech.*, **42**(2), 229-245.
- Simon, D. (2006), *Optimal state estimation – Kalman, H<sub>∞</sub>, and nonlinear approaches*, John Wiley & Sons Inc., Hoboken, NJ.
- Smyth, A. and Wu, M. (2007), "Multi-rate Kalman filtering for the data fusion of displacement and acceleration response measurements in dynamic system monitoring", *Mech. Syst. Signal Pr.*, **21**(2), 706-723.
- Tamura, Y., Matsui, M., Pagnini, L.C., Ishibashi, R. and Yoshida, A. (2002), "Measurement of wind-induced response of buildings using RTK-GPS", *J. Wind Eng. Ind. Aerod.*, **90**(12-15), 1783-1793.
- Trifunac, M.D. (1971), "Zero baseline correction of strong motion accelerograms", *B. Seismol. Soc. Am.*, **61**(5), 1201-1211.
- Wang, N., O'Malley, C., Ellingwood, B.R. and Zureick, A.H. (2011), "Bridge rating using system reliability assessment. I: Assessment and verification by load testing", *J. Bridge Eng.*, **16**(6), 854-862.
- Yang, H., Takaki, T. and Ishii, I. (2012), "Real-time multidirectional modal parameter estimation of beam-shaped objects using high-speed stereo vision", *Proceedings of IEEE, Sensors*, Taipei, Taiwan.
- Yun, X., Calusdian, J., Bachmann, E.R. and McGhee, R.B. (2012), "Estimation of human foot motion during normal walking using inertial and magnetic sensor measurements", *IEEE T. Instrum. Meas.*, **61**(7), 2059-2072.
- Zhou, C., Li, H., Li, D., Lin, Y. and Yi, T. (2013), "Online damage detection using pair cointegration method

- of time-varying displacement”, *Smart Struct. Syst.*, **12**(3-4), 309-325.
- Zhu, L. (2003), “Recovering permanent displacements from seismic records of the June 9, 1994 Bolivia deep earthquake”, *Geophys. Res. Lett.*, **30**(14), doi:10.1029/2003GL017302, 14.